A finite element study on the effect of curvature on the reinforcement of matrices by randomly distributed and curved nanotubes

Christian Diedrich[1], Dirk Dijkstra[1], Jan Hamaekers*[2], Bjoern Henninger[1], and Maharavo Randrianarivony[2]

[1]Bayer MaterialScience AG, Leverkusen, Germany
[2]Fraunhofer Institute for Algorithms and Scientific Computing SCAI, Sankt Augustin, Germany

May 13, 2014

Abstract

A significant reinforcement effect has always been expected from the use of carbon nanotubes (CNT). Well-known experimental results, however, reveal that the theoretical reinforcement rules for straight nanotubes are not always achieved in practice. This paper reports that not only should the percentage quantity of nanotubes in the matrix be taken into account, but also their curvatures. A finite element method (FEM) based computational analysis on the mechanical reinforcement of composite materials by nanotubes is presented. In this article we focus on randomly distributed and curved nanotubes as fillers. In particular, we study the influence of the curvature of the nanotubes on the overall elastic moduli. To this end, we apply a statistical analysis of the elastic moduli of nanocomposites when a certain number of nanotubes are incorporated into a matrix. Here, we restrict ourselves to use just a simple as possible linear elasticity model. Nevertheless, it turns out that the average overall reinforcement ratio is significantly lower than in the case of aligned straight nanotubes. In particular, our numerical experiments show that the resulting reinforcement ratios exhibit a linear dependency on the average ratio of the end-to-end distance and the length of the nanotube.

Keywords: Finite Element Analysis, Reinforced Nanocomposites, Curved Nanotubes, Young's Modulus

*jan.hamaekers@scai.fraunhofer.de

1 Introduction

Nanotechnology is a very important field which has emerged in recent decades and has very rapidly evolved in several different directions simultaneously. Nanotechnology has important applications in many fields such as aviation, automobiles, electronics and medical engineering. In particular, nanocomposite materials have various important properties, e.g. electronic, thermal and mechanical, which can be exploited in many areas of application [1–3]. In this work, we are interested in the mechanical reinforcement of nanomaterials based on nanotubes. Here, many theoretical studies predict that the use of nanotubes as fillers will result in a substantial reinforcement of the matrix [4–10]. Experimental data in the literature indicate that in certain material systems a significant reinforcement may be possible with the use of only a small percentage of nanotubes [1, 11, 12]. However, experimental results on several thermoplastic and thermoset matrices show that the reinforcement ratios actually achieved are generally substantially less. To our knowledge, this behavior has so far not been described by theoretical models, e.g. by conventional rules of mixtures. For example, let us consider a material consisting of two components (fiber and matrix), assuming E_f and E_m as the respective Young's moduli. In that case, the simplest rules of mixture for the Youngs modulus of the composite material are the well-known rules of Voigt and Reuss, which are also called the direct and inverse rules of mixture [13]. The direct rule of mixture reads

$$E_1 = E_f V_f + E_m V_m \tag{1}$$

and among other things gives an upper boundary for the total modulus, while the inverse rule reads

$$E_2 = E_f E_m / (E_m V_f + E_f V_m) \tag{2}$$

and gives a lower boundary [13]. Here, V_f and V_m are the volume fractions of the fiber and the matrix with respect to the total volume of the composite material. However, in many cases these simple rules fail and hence several much more sophisticated rules of mixtures have been proposed. Hu et al. give a good survey [13] of the most frequently applied rules of mixtures. In particular, stiffness and strength enhancements achieved by the use of fillers of different shapes such as cylinders and disk-like platelets are examined. It should be noted that in case of general composite materials, rules of mixtures are usually not sufficient to predict the reinforcement. In those cases, finite element method (FEM) based computations provide a theoretical prediction method. A comparison of the FEM solution with experimental results is given by Lee et al. in [14], which is interested primarily in metal matrix composites. In addition, they compare their results with the Halpin-Tsai rule of mixtures [15]. A statistical study is conducted by Hbaieb et al. in [16]. They also perform a comparison of aligned tubes with randomly positioned, unorganized straight tubes. In their analytical investigation they compare their results with the Mori-Tanaka rule of mixture [17]. Curved nanotubes have also been considered by some authors. In

this regard, Shi et al. [18] used a helical spring shape and Brinson et al. [19, 20] a sinusoidal shape in the framework of the Mori-Tanaka model. Furthermore, a mixed numerical-analytical model for nanotube-reinforced nanocomposites also using sinusoidal shaped nanotubes was presented by Pantano in [21]. Here, the correlation matrix needed for the Mori-Tanaka model is determined by finite element analysis computations. Recently, Han et al. [22, 23] introduced a geometric model which includes interphase regions and also agglomeration and clusterization of carbon nanotubes (CNT). Moreover, a methodology for the reconstruction of carbon nanotube composite microstructure using correlation cunctions was presented in [24].

Expectations for the reinforcing effect of CNT were tremendous. These ultra-high-modulus tubes with a length of up to several micrometers and a diameter of only several nanometers should, due to the good load transfer action of these large surface area fillers, have a tremendous reinforcing effect, as calculated by means of the well-known reinforcement rules. Traditionally, short-fiber reinforcement always meant reinforcement by means of straight fibers because glass, Kevlar, carbon and even whiskers are always straight. For most commercial polymers, the experimentally identified reinforcing effect of CNTs in polymers is much less than calculated from composite theory, i.e. either the modulus of these fibers is much lower than expected or the stress transfer (adhesion) is inhibited or we are using the wrong theory. This paper elucidates the influence of the curvature of the fibers on the reinforcing effect. Some examples of large reinforcing effects are reported in the literature, but these results can be explained by other than fiber reinforcement [4, 25].

Note that up to our knowledge the specific effect of curvature on the reinforcement ratio has not been specifically studied in the case of more arbitrarily and randomly curved nanotubes so far. Therefore, in this work, we study the mechanical properties of matrices with randomly distributed and curved nanotubes by means of a finite element analysis to obtain more detailed insight on the impact of curvature from a theoretical point of view. Here, we focus on the case of the reinforcement of high-modulus matrices. To this end, we restrict ourselves to a simple as possible linear elasticity model, where we in particular neglect interphase regions. This way a perfect load transfer and no reinforcement effect of the filler on the mechanical properties of its local neighboring matrix is assumed. In addition, we compare analytic rules of mixtures and our results of FEM simulations. It turns out that the reinforcement ratio achieved using curved nanotubes as fillers is significant lower than in the case of straight nanotubes. Furthermore, our results show a linear dependency of the reinforcement ratio on the average ratio of the end-to-end distance and the length of the nanotube.

The body of this paper is organized as follows: In Section 2, we briefly review the experimental study performed for reinforced epoxy resin which motivated this work. In Section 3 we briefly summarize the finite element approach to compute elastic moduli based on linear elasticity. In Section 4 we present various numerical experiments and discuss their results. Finally, we offer some concluding remarks in Section 5.

2 Experiment

As mentioned above, the computational study presented in this article was primarily motivated by the results of experimental investigations on CNT modified epoxy resins. Experimental results on typical epoxy resins reinforced with multi-walled carbon nanotubes (MWCNT) show that the reinforcement ratio is much less than predicted from the rule of mixtures. This brief experimental section summarizes the experimental setup and some of the typical results.

Table 1: Results of experimental study on epoxy CNT composites with increasing weight-% of CNTs.

weight-%	E/E_m	Std. dev.
0.0	1.000	0.039
0.5	1.049	0.029
1.0	0.990	0.029
1.5	1.020	0.029
2.0	1.029	0.029
2.3	1.000	0.020
25.9	1.147	0.069

To illustrate a typical experimental setup, we included data for a typical epoxy matrix reinforced by MWCNT. The C150P Baytubes used were chemically surface-modified to facilitate the chemical bonding of the CNT to the epoxy resin. The resulting CNT were dispersed into RIM135 epoxy resin from Momentive using a three-roll-mill. The resulting master batch contained 3 weight-% modified CNT. Using this master batch, several mixtures of different CNT content with RIM135 resins were produced . These samples were cured using the hardener RIM H137 in a ratio of 100 : 30 and at temperature of 50° C for 5 h followed by a post-curing cycle at 75° C for 6h. The modulus of elasticity of the epoxy matrix is 2.9 ± 0.2 GPa. The sample containing approximately 26 wt-% CNT had been produced using a different experimental method. The CNT in agglomerated form was filled into a mold and the resin-hardener mixture was infused into the agglomerates using a modified VA-RTM process. The cured composites were cut and tested in a 3-point bending set-up according to ISO 178. The results are presented in Table 1 and show a substantially lower reinforcement ratio than expected from the rule-of-mixtures or as found in the literature for certain low-modulus matrices where, for example, an increase in the elastic modulus of up to 40% is reported for 1% MWNT in polyester resin, and an increase of up to 400% of is reported for 20% single-wall carbon nanotubes (SWNT) in polyethylene ($E \approx 0.1 - 1.2$ GPa) [1, 11, 12].

3 Numerical methods

For the computation of the Youngs modulus of the composite material by means of a finite element analysis, we use the FEM code OOF2 [26–28], where we assume that the matrix and the fiber materials are linearly and isotropically elastic. Hence, the Young's modulus and the Poisson ratio are sufficient to fully specify the material properties. As discussed in the introduction, we do not include interphase regions and assume that the fibers are perfectly bonded to the matrix. For reasons of simplicity we further restricted ourselves to a 2D finite element model which is subjected to plane stress. Note that of course a 3D model allows to compute quantitative better results compared to the 2D model. However, a 2D model is usually sufficient to give qualitative statements [16], which is the main purpose of our work. Now, to perform a uniaxial tensile load test we use symmetrical boundary conditions as described in [16]. Here, a uniform strain is applied in x direction of the composite material by specific Dirichlet boundary conditions. This is done by applying a constant displacement δ to the x-component of the right boundary, while the x-component of the left side and the y-component of the bottom boundary is kept fixed to zero. Note that the y-components of the left and right boundary and the x-component of the bottom boundary are not fixed and hence are still allowed to vary. Compare also the illustration in Figure 1(a). The elastic moduli are then calculated according to a generalized Hookes law [29], i.e. by dividing the respective computed averaged stress components by the respective strain components [8, 9]. For example, the Young's modulus E_{xx} resulting from a longitudinal tensile load test is given by

$$E_{xx} = \frac{\sigma_{xx}}{\epsilon_{xx}},$$

where σ_{xx} and ϵ_{xx} denote the average stress and strain component, respectively. In our case, the applied strain is $\epsilon_{xx} = 0.1$, where the average stress component is given by the integral of the respective FEM based computed local stress component over the computational domain divided by the area value of the computational domain. Let us note that we can use here quite a large strain value, like e.g. $\epsilon_{xx} = 0.1$, since we use a linear elasticity model and hence the resulting elastic constant is independent of the value of the applied strain except up to numerical artifacts. In Figure 1(b) we give an example for an instance of a finite element mesh for a nanocomposite including several curved nanotubes with an aspect ratio of $1 : 50$. A snapshot of a uniaxial tensile load test for a single curved tube embedded in a matrix is presented in Figure 1(c). Here, the computed local value of the stress component σ_{xx} is represented by the color scale displayed.

For validation, we applied our FEM approach to several test cases, where the exact solution is given by a certain rule of mixtures. For example, we considered simple composite material where the well-known direct and inverse rules of mixture, c.f. equations (1) and (2), give the exact Young's modulus of the composite material [13].[1] In addition, we considered oriented unidirectional

[1] Here, in particular, we investigated also the effect of the application different strain values,

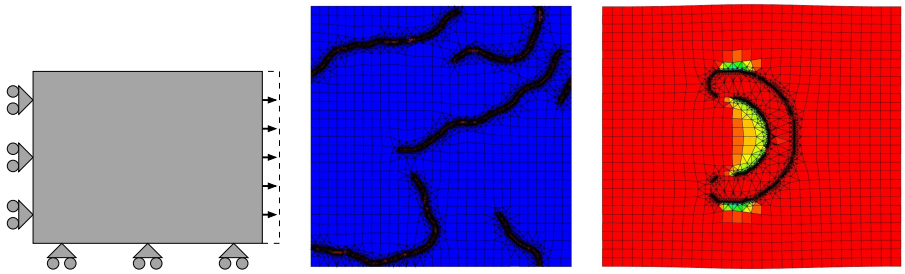

(a) (b) (c)

Figure 1: (a) Schematic view of an uniaxial tensile load case. (b) FEM mesh for nanotubes embedded in a matrix. (c) Numerical FEM results of an uniaxial tensile load test of a single curved tube.

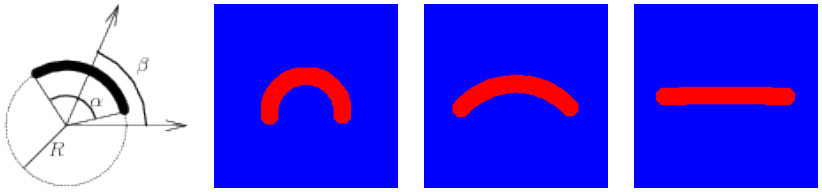

(a) (b) (c) (d)

Figure 2: Single curved tubes, where the volume fractions are kept constant and only the curvatures of the internal models change.

fibers, in cases of the special rules given in [30], such as the shear lag rule of mixture $E = \eta_L V_f E_f + (1 - V_f)E_m$, where the parameter η_L depends on the specific arrangements. Here, and also in the case of the Halpin-Tsai rule, our results agree well with the known theoretical results. But however, for reasons of simplicity, we will not give further details here.

4 Numerical simulations and results

4.1 Single curved fiber

This article is primarily concerned with the numerical simulation of curved nanotubes. Therefore, to get a first insight on the effect of curvature on reinforcement in general, below we discuss the simplest imaginable curved models embedded in a matrix. Here, the principal objective is to investigate the influ-

i.e. we compared several values in the range of 1% to 10%. As expected it turned out that the resulting Young's moduli are independent of the used strain value except up to numerical noise.

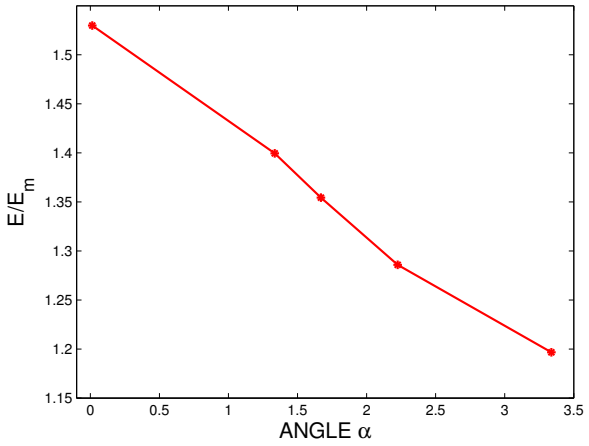

Figure 3: Reinforcement ratios for samples according to Figure 2 for horizontal uniaxial load test cases. The length is kept constant $L = 133.52$. The moduli are set to $E_m = 1$ and $E_f = 100$. The Poisson ratios are $\nu_m = \nu_f = 0.33$.

ence of the geometric properties including curvature. In other words, we keep the volume fraction constant throughout the following computations. The only parameters that vary are the shape of the fiber as well as its rotation with respect to the uniaxial load direction. It should be noted that in the case of fixed moduli E_f and E_m and a fixed volume fraction V_f, the simple direct and inverse rule of mixtures fail since they remain constant. The primary models to be considered are straight segments and circular arcs, assuming three controlling parameters α, β, R as in Figure 2(a). The parameter α controls the spanning angle of the circular arc which is traced on a circle of radius R while the parameter β expresses the rotational angle with respect to the horizontal axis.

First, we consider circular arcs which are oriented horizontally, i.e. the angle β is constantly zero as illustrated in Figure 2. The spanning angles α are allowed to vary and the end-to-end distances are chosen such that the arc lengths $L = \alpha R$ are constant. The effect of the reinforcement is depicted in terms of the factors of variation in Figure 3. It can be observed that the reinforcement ratio is inversely proportional to the spanning angle α. In particular, the obtained ratio reaches its maximal value of about 1.53 and its minimal value of about 1.12 at $\alpha = 0$ and $\alpha = \pi$, respectively. Note that the resulting ratios are substantially lower than the value computed by the direct rules of mixtures, i.e. $E_1 \approx 8.1$. Let us further remark that the lower bound is given by the inverse rules of mixtures, i.e. $E_2 \approx 1.08$.[2]

[2]Note that there are small deviations E_1 and E_2 with respect to the different samples caused by minor inaccuracies of the pixel in the FEM images which are unavoidable for

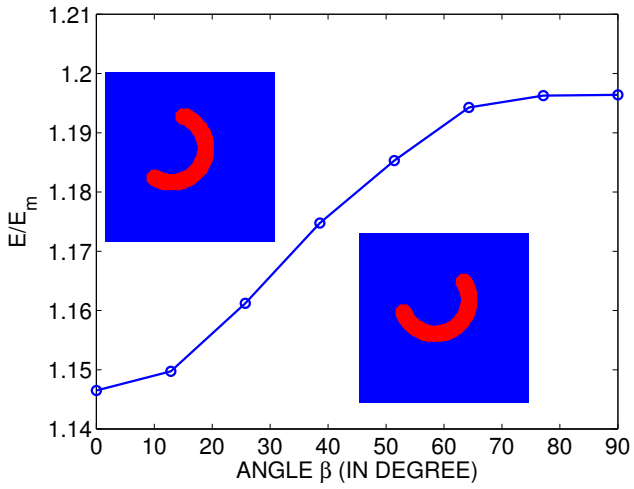

Figure 4: Circular arc by varying $\beta \in [0, 90]$ degree using fixed $E_m = 1.0$, $E_f = 100.0$ and $\nu_m = \nu_f = 0.3333$. The volume and the shape are kept constant, i.e. end-to-end distance of a value of 79.6.

Let us now consider the influence of the rotation angle β on the reinforcement ratio. More precisely, a fixed curved tube in the form of a circular arc of fixed radius and fixed spanning angle α is allowed to rotate inside a matrix. The behavior of the dependence of the reinforcement in term of the rotational angle β is plotted in Figure 4.

Altogether, the investigation proposes that the results from straight tubes cannot be directly applied to curved and rotated tubes. While the direct and inverse rules of mixture are very efficient in the case of vertical and horizontal straight tubes [30], they are altogether incapable of providing a reliable prediction for curved and rotated nanotubes.

4.2 Multiple nanotubes

In this section we consider the case of multiple randomly distributed and curved nanotubes embedded in a matrix. To generate such nanocomposites we apply an approach based on particle dynamics. In detail, we model a nanotube as a linear chain of pseudo-particles which interact by static harmonic bond potentials i.e.

$$U(r) = k_B(r - r_0)^2,$$

and static harmonic angle potentials, i.e.

$$U(\theta) = \frac{k}{2} \cdot (\cos(\theta) - \cos(\theta_0))^2 .$$

curved fibers.

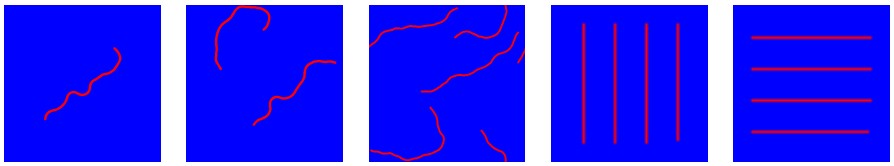

(a) (b) (c) (d) (e)

Figure 5: Samples of nanocomposites: (a), (b), (c) curved nanotubes, (d) vertical straight nanotubes, (e) horizontal straight nanotubes. The aspect ratio of a nanotube is $1 : 50$.

We use the following fictitious values for the static bond $k_B = 191.637$, $r_0 = 1.54$, $k = 1000$ and for the angle potentials we choose $\cos(\theta_0) = -1$ and $k = 1000$.[3] Additionally, in order to avoid crossings between different nanotubes, we apply a standard Lennard-Jones potential between pseudo-particles of different nanotubes. The corresponding numerical simulations are performed by the molecular dynamics software package Tremolo-X [31]. Here, we applied an NVT ensemble using a Verlet time integrator with a time step of 0.1 for the Verlet time integrator and a Berendsen thermostat with a fictitious target temperature 0.1. Note that since we are considering only pseudo-particles, all the indicated values have no physical meaning and are dimensionless, but we can control the average curvature (or how straight the nanotubes are) by the choice of the bond angle parameter k. To generate a series of samples to a specific set of model parameters, we take snapshots every 10000 time steps during a simulation run.

Now, in a first step, we analyze the reinforcement factor as a function of the number of curved nanotubes. Note that we restrict ourselves to the case of model materials with fictitious materials parameters. However, we consider typical fiber/matrix moduli ratios in nanotube composites. Note further that we investigated also the effect of different Poisson ratios by numerical simulation. But since our results showed only a very small influence, we restrict ourselves to the case of equal Poisson ratios for fibers and matrix in this work. In our computations, we use an aspect ratio of $1 : 50$ for the curved as well as the vertical/horizontal arrangements.

Before considering a large number of samples of nanocomposites, we consider first the individual samples illustrated in Figure 5. In fact, we consider three simulations using respectively one, two and four nanotubes.

Here, we first fix E_m and let E_f vary. Afterward, the converse is executed by fixing E_f and varying E_m. The corresponding results of the tests are displayed in Figure 6(a), Figure 6(b) and Figure 6(c). It can be seen that for each test, the two curves align well. In other words, the reinforcement ratios E/E_m of the considered sample systems depend only on the ratio E_f/E_m. In the follow-

[3]Note that since we are considering only pseudo particles, all the indicated values have no physical meaning and are dimensionless

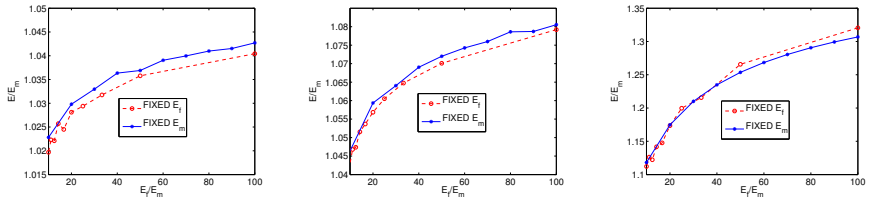

(a) (b) (c)

Figure 6: Computed reinforcement ratios: (a) one nanotube, (b) two nanotubes, (c) four nanotubes. The aspect ratio of a nanotube is 1 : 50.

ing we always use elastic moduli $E_m = 1.0$ and $E_f = 100.0$, and the Poisson ratio $\nu_m = \nu_f = 0.3333$. By observing these three plots more closely, we see that the reinforcement increases proportionally with the number of nanotubes, but no conclusions can yet be derived because these were only individual tests. Therefore, for each case, i.e. the cases of 1, 2, 3, 4 nanotubes, we performed simulations on 90 different samples of nanocomposites. The results are summarized in Figure 7, where the points in the figure represent the different computed reinforcements of the individual tests while the horizontal lines depict their average values.

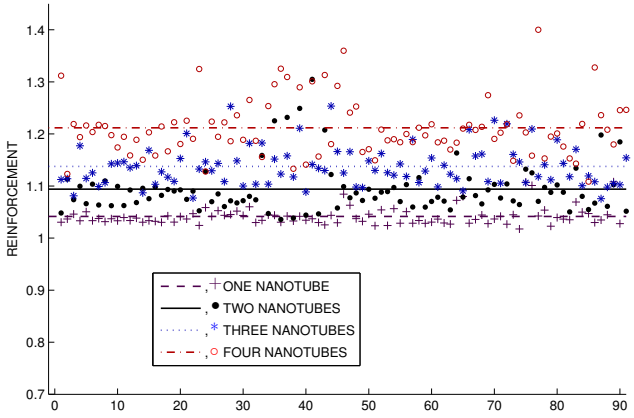

Figure 7: Computed reinforcement ratios of samples of nanocomposites embedding one, two, three and four nanotubes, respectively. The samples are generated by our particle dynamics approach. We use the elastic moduli $E_m = 1.0$ and $E_f = 100.0$, and Poisson ratio $\nu_m = \nu_f = 0.3333$. The aspect ratio of a nanotube is 1 : 50.

Furthermore, in Figure 8(a) we give the averaged reinforcement ratios in

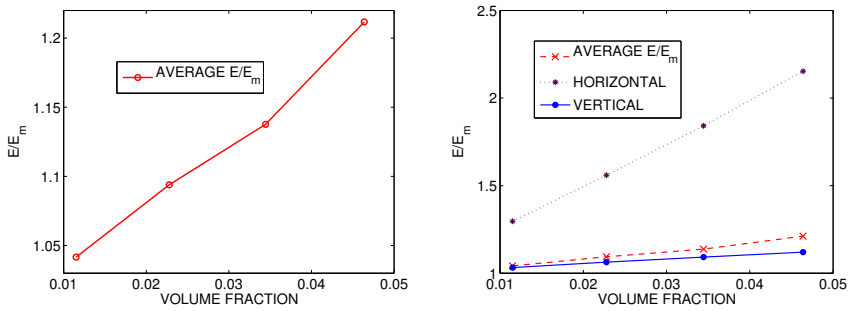

(a) (b)

Figure 8: (a) Average reinforcement ratios using 1, 2, 3 and 4 curved nanotubes, (b) Computed reinforcement ratios for horizontal and vertical nanotube samples according to Figure 5(e) and Figure 5(d).

terms of the volume fraction of the nanotubes and it can be seen that there is an almost linear dependency. In addition, we compare the case of curved nanotubes with the two extreme cases which consist of vertical and horizontal nanotubes as shown in Figure 5(d) and Figure 5(e) respectively. Figure 8(b) illustrates the average reinforcement ratio of the curved nanotubes together with the extreme cases. The entire numerical results are organized in Table 2. In

Table 2: Average values of the E/E_m according to the samples of Figure 7. In addition we give the results of the extreme cases 5(d) and 5(e), and the direct and inverse rule of mixtures.

# NT	V_f	E/E_m	Horiz. (E/E_m)	Vert. (E/E_m)	E_1	E_2
1	0.01	1.04	1.30	1.03	2.139	1.012
2	0.02	1.09	1.56	1.06	3.255	1.023
3	0.03	1.14	1.84	1.09	4.409	1.035
4	0.05	1.21	2.15	1.12	5.593	1.048

particular, we see that the reinforcement ratios for these model cases are in the range the ratios we measured experimentally.

Let us now study the effect of the curvature ratio $\delta = \ell/L$, where ℓ is the end-to-end distance of the nanotubes and L represents the chordal length. A small curvature ratio corresponds to nanotubes that are very floppy as illustrated in Figure 9(a), while a high curvature ratio represents a nanotube which is very elongated as it approaches a straight nanotube as illustrated in Figure 9(b).

To examine the influence of the curvature ratio on the reinforcement ratio of the nanocomposite, we first generate different sets of samples of nanocomposites

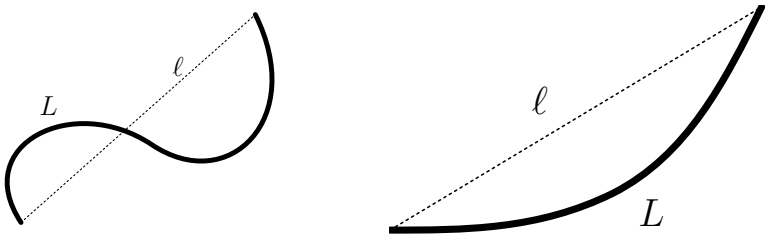

(a) (b)

Figure 9: Curved nanotubes and the parameters for the curvature computation: (a) floppy tube, (b) elongated tube.

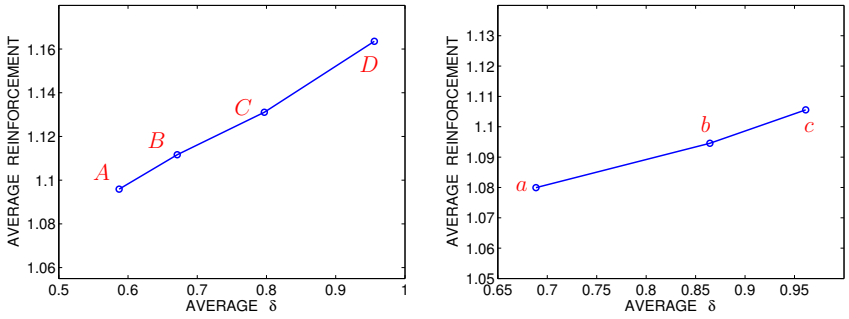

(a) (b)

Figure 10: Dependence of the reinforcement factors on the curvature ratios: (a) two long tubes, (b) four short tubes.

which exhibit different average curvature parameters δ. To this end, we apply our particle dynamics approach with different values k for the bond angle potential, i.e. $k = 10^3$, $k = 10^4$, $k = 10^5$ and $k = 10^6$, where we restrict ourselves to samples with just two nanotubes of the same chordal length. We identify the resulting four sets of samples as sets A, B, C and D, respectively. We present the resulting average curvature ratios in Figure 11, where the average curvature ratios increase from datasets A to D. In Figure 12, we present all the individual measurements of the reinforcement ratio as well as the average values for the datasets A, B, C and D.

The simulation results reveal that the average curvature ratio really does have an influence on the elastic modulus of the nanocomposite. Although the reinforcement values are scattered, it can be observed that their average values increase proportional to the values of the curvature parameters. A more accurate description of that dependence is displayed in Figure 10(a). In Table 3 we collect the statistical data corresponding to the former measurements. In particular,

we use the standard deviation $\left[\sum_{i=1}^{n}(x_i-\bar{x})^2/n\right]^{1/2}$ and its squared value which is the variance. We also show the average absolute deviations $\sum_{i=1}^{n}|x_i-\bar{x}|/n$. Here we use the absolute evaluation of the deviations from the average values $\bar{x}$. It can be noticed that as the number of inserted nanotubes increases, the value of the deviations increases as well. Moreover, we observe that a data set with an average low curvature ratio has small standard deviations in the reinforcement factors. Similar deviation statistics for the other measurements are presented in Table 4 and Table 5. In particular, it can be observed that smaller values of the curvature parameter δ correspond to larger standard deviations. That is because they are more susceptible to distortion by straight segments.

Table 3: Statistical values of the measurements for Figure 7, that is the mean value, the standard deviation, the variance and the average absolute deviation.

DATA	Mean val.	Std. dev.	Variance	Avr. abs. dev.
One nanotube	1.042	0.017	0.0003	0.012
Two nanotubes	1.094	0.047	0.0022	0.031
Three nanotubes	1.138	0.038	0.0015	0.030
Four nanotubes	1.212	0.055	0.0030	0.041

In a next step, we consider additional sets of samples, namely a, b and c, which are similar to the first sets, i.e. A, B, C and D, with two exceptions. First, there are now twice as many (i.e. now four internal curved tubes). Second, the length of the tubes is now half as long as the previous ones, i.e. with the same volume content. In Figure 10(b), we omit the intermediate results and show only the average dependence of the material reinforcements on the values of the curvature parameter δ. The three datasets (a, b, c) correspond to the three dots of the plot in Figure 10(b). Once again, we can observe the linear behavior of the reinforcement as a function of the curvature ratio. That suggests that not only the aspect ratio but also the curvature values are on average significant in the estimation of the reinforcement ratio.

Table 4: Statistical values according to the computed average reinforcement ratios E/E_m presented in Figure 12, that is the mean value, the standard deviation, the variance an the average absolute deviation.

DATA	Mean val.	Std. dev.	Variance	Avr. abs. dev.
A	1.096	0.034	0.0012	0.028
B	1.112	0.053	0.0028	0.043
C	1.131	0.066	0.0044	0.051
D	1.164	0.125	0.0157	0.096

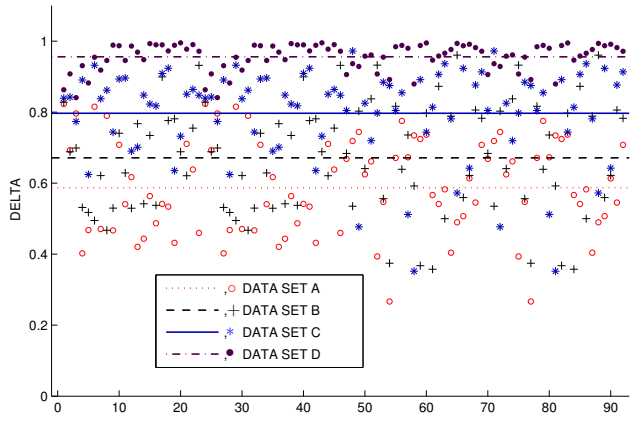

Figure 11: Average curvature ratios for sample sets A, B, C and D.

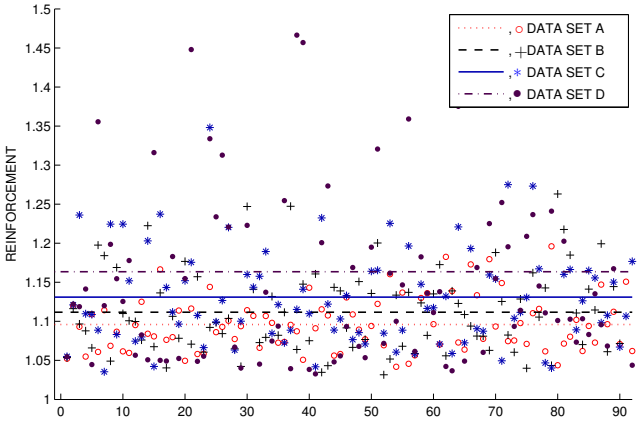

Figure 12: Computed average reinforcement ratios for the sets A, B, C and D admitting increasing curvature ratios.

Table 5: Statistical values according to the computed average curvature parameters δ presented in Figure 11, that is the mean value, the standard deviation, the variance and the average absolute deviation.

DATA	Mean val.	Std. dev.	Variance	Avr. abs. dev.
A	0.587	0.139	0.0192	0.118
B	0.671	0.153	0.0234	0.130
C	0.797	0.130	0.0168	0.098
D	0.956	0.039	0.0015	0.031

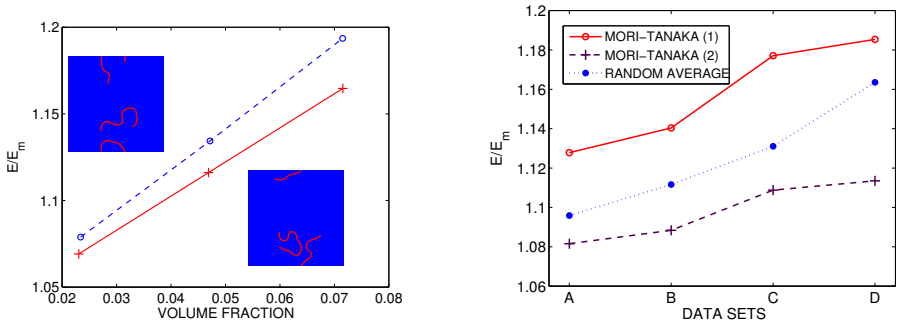

(a) (b)

Figure 13: (a) Computed reinforcement ratios with increasing aspect ratios. (b) Mori-Tanaka prediction for data sets A, B, C and D.

We have also performed computations pertaining to the influence of the thickness in the case of curved tubes. Let us now focus on the case in which the curvature parameter δ is fixed. To do that, we considered two composite materials that consist of two internal curved nanotubes. The results of the computation are depicted in Figure 13(a), where the thickness can be determined from the volume fraction in the horizontal axis. In all our simulations, the postures and positions of the internal nanotubes are kept invariant. The only variations we allowed were the aspect ratios as the quotient between the thickness and the chordal length of the embedded nanotubes. As the aspect ratio increases, the volume fractions of the fiber with regard to the matrix increase as well. In both cases, we observed the linear dependence of the average reinforcement ratio on the nanotube volume fractions.

Finally, we perform numerical simulations with regard to the Mori-Tanaka rule of mixtures [17, 32, 33]. We consider randomly placed curved nanotubes inside a matrix [14] and we examine the average behavior with respect to the Mori-Tanaka estimation. The results presented are not based on analytical

methods but rather on numerical simulation, where the samples are generated by our particle dynamics approach. Briefly, the Mori-Tanaka prediction as surveyed in [13] expresses the estimation in term of the overall bulk and share moduli K and μ. The estimation is produced in function of the properties K_f and μ_f of the fibers and those of the matrix K_m and μ_m. More specifically, the bulk estimate is

$$K = K_m + K_m V_f \varphi / (1 - V_f(1 - \alpha)),$$

where parameters φ and α depend on the specific structure of the nanocomposite. The shear modulus is estimated in a similar manner. The exact dependence of the parameters, which is not repeated here, is found in [32]. The principal expression in that dependence is a certain parameter $\chi = c/a$ (see expression (12) in [32]) which is usually proportional to the quotient between the average width of the fibers c and the average length a. We have applied the former sample sets A, B, C and D to the Mori-Tanaka prediction. Our simulation reveals that using χ without taking the curvature parameter δ into account provides a value of approximately 1.30 for all four datasets A, B, C and D. In other words, for curved nanotubes, using only the aspect ratio between the width and the chord length of the curved nanotubes does not provide a reliable estimate of the material properties, because it cannot detect the increase of the average reinforcement as the value of the curvature parameter increases such that $\delta_A < \delta_B < \delta_C < \delta_D$. On the other hand, we have observed that replacing χ by an order $\mathcal{O}(\chi/\delta)$ yields a reasonable estimate in the Mori-Tanaka prediction. In fact, we performed additional investigations by including the value of δ inside the value of χ such as $\chi = \lambda c(\delta\alpha)$ where λ is a factor and c/α is as before the aspect ratio. As a result, we obtain much better estimates where the increase of the reinforcement in the datasets can be detected. We have not yet been able to determine the optimal value for the factor λ but the dependence on the inverse of δ is captured. In Figure 13(b), we consider two cases where $\lambda_1 = 0.5$ and $\lambda_2 = 0.25$ in which the Mori-Tanaka estimates for these values increase with respect to the sets A, B, C and D. In the same figure, we have re-plotted the average reinforcement ratio which we took from Figure 10(a) for the sake of comparison. For both values of the factor λ, the results exhibit increasing plots as the average reinforcement increases.

5 Conclusions

The results of the numerical simulations show that the curvature of the nanotubes has an impact on the ratio of reinforcement of the matrix. Indeed, our numerical results exhibit a linear dependency of the reinforcement ratio on the curvature parameter introduced. Furthermore, our results suggest that the Young's modulus of CNT reinforced high-modulus matrices can be predicted by linear elasticity based FEM, while the experimentally observed relative high reinforcement ratios in the case of low-modulus epoxy matrices cannot be reproduced by a standard linear elasticity based FEM model. This may further

suggest that in the case of low-modulus epoxy matrices the structural morphology of the matrix is modified by the inclusion of nanotubes.

References

[1] L. Brand, M. Gierlings, A. Hoffknecht, V. Wagner, and A. Zweck. Kohlenstoff-Nanoröhren: Potenziale einer neuen Materialklasse für Deutschland. *VDI-Technologiezentrum, Düsseldorf*, 79, 2009.

[2] T. Borca-Tasciuc, M. Mazumder, Y. Son, S. Pal, L. Schadler, and P. Ajayan. Anisotropic thermal diffusivity characterization of aligned carbon nanotube-polymer composites. *Journal of Computational and Theoretical Nanoscience*, 7:1581–1588, 2007.

[3] M. Mazrouei, H. Jokar, M. Baniassadi, K. Abrinia, and M. Haghighi-Yazdi. Evaluating the effect of mechanical loading on the effective thermal conductivity of CNT/polymer nanocomposites. *Journal of Computational and Theoretical Nanoscience*, 11(8):1738–1744, 2014.

[4] J. Coleman, U. Khan, W. Blau, and Y. Gun'ko. Small but strong: a review of the mechanical properties of carbon nanotube–polymer composites. *Carbon*, 44(9):1624–1652, 2006.

[5] M. Shokrieh and R. Rafiee. A review of the mechanical properties of isolated carbon nanotubes and carbon nanotube composites. *Mechanics of Composite Materials*, 46(2):155–172, 2010.

[6] J. Robertson. Realistic applications of CNTs. *Materials Today*, 7(10):46–52, 2004.

[7] Y. Han and J. Elliott. Molecular dynamics simulations of the elastic properties of polymer/carbon nanotube composites. *Computational Materials Science*, 39(2):315–323, 2007.

[8] M. Griebel, J. Hamaekers, and F. Heber. A molecular dynamics study on the impact of defects and functionalization on the Young modulus of boron–nitride nanotubes. *Computational Materials Science*, 45(4):1097–1103, 2009.

[9] M. Griebel and J. Hamaekers. Molecular dynamics simulations of the elastic moduli of polymer–carbon nanotube composites. *Computer Methods in Applied Mechanics and Engineering*, 193(17):1773–1788, 2004.

[10] N. Nouri and S. Ziaei-Rad. Mechanical property evaluation of buckypaper/epoxy composites using molecular dynamics simulations fully implemented on graphical processing units. *Journal of Computational and Theoretical Nanoscience*, 9(12):2144–2154, 2012.

[11] E. Barrera, M. Shofner, and E. Corral. Applications: Composites. In M. Meyyappan, editor, *Carbon Nanotubes: Science and Applications*, pages 321–351. CRC press, 2004.

[12] D. Qian, E. Dickey, R. Andrews, and T. Rantell. Load transfer and deformation mechanisms in carbon nanotube-polystyrene composites. *Applied Physics Letters*, 76:2868–2870, 2000.

[13] H. Hu, L. Onyebueke, and A. Abatan. Characterizing and modeling mechanical properties of nanocomposites-review and evaluation. *Journal of Minerals & Materials Characterization & Engineering*, 9(4):275–319, 2010.

[14] W. Lee, J. Son, N. Kang, I. Park, and Y. Park. Finite-element analysis of deformation behaviors in random-whisker-reinforced composite. *Scripta Materialia*, 61(6):580–583, 2009.

[15] J. Halpin and J. Kardos. The Halpin-Tsai equations: a review. *Polymer Engineering & Science*, 16(5):344–352, 1976.

[16] K. Hbaieb, Q. Wang, Y. Chia, and B. Cotterell. Modelling stiffness of polymer/clay nanocomposites. *Polymer*, 48(3):901–909, 2007.

[17] T. Mori and K. Tanaka. Average stress in matrix and average elastic energy of materials with misfitting inclusions. *Acta Metallurgica*, 21(5):571–574, 1973.

[18] D. Shi, X.Q-Feng, Y. Huang, K.-C. Hwang, and H. Gao. The effect of nanotube waviness and agglomeration on the elastic property of carbon nanotube-reinforced composites. *Journal of Engineering Materials and Technology*, 126:250–257, 2004.

[19] F. Fisher, R. Bradshaw, and L. Brinson. Fiber waviness in nanotube-reinforced polymer composites–I: Modulus predictions using effective nanotube properties. *Composites Science and Technology*, 63(11):1689–1703, 2003.

[20] R. Bradshaw, F. Fisher, and L. Brinson. Fiber waviness in nanotube-reinforced polymer compositesii: modeling via numerical approximation of the dilute strain concentration tensor. *Composites Science and Technology*, 63(11):1705–1722, 2003.

[21] A. Pantano. Numerical–analytical model for nanotube-reinforced nanocomposites. In V. Mittal, editor, *Modeling and Prediction of Polymer Nanocomposite Properties*, pages 201–214. John Wiley & Sons, 2012.

[22] F. Han, Y. Azdoud, and G. Lubineau. Computational modeling of elastic properties of carbon nanotube/polymer composites with interphase regions. Part I: Micro-structural characterization and geometric modeling. *Computational Materials Science*, 81:641–651, 2014.

[23] F. Han, Y. Azdoud, and G. Lubineau. Computational modeling of elastic properties of carbon nanotube/polymer composites with interphase regions. Part II: Mechanical modeling. *Computational Materials Science*, 81:652–661, 2014.

[24] D. Li, M. Baniassadi, H. Garmestani, S. Ahzi, M. Reda Taha, and D. Ruch. 3D reconstruction of carbon nanotube composite microstructure using correlation functions. *Journal of Computational and Theoretical Nanoscience*, 7(8):1462–1468, 2010.

[25] J. Coleman, M. Cadek, R. Blake, V. Nicolosi, K. Ryan, C. Belton, A. Fonseca, J. Nagy, Y. Gun'ko, and W. Blau. High performance nanotube-reinforced plastics: understanding the mechanism of strength increase. *Advanced Functional Materials*, 14(8):791–798, 2004.

[26] R. Garcıa, C. Bishop, W. Carter, S. Langer, P. Limthongkul, and Y. Chiang. Microstructural modeling and design of rechargeable lithium-ion batteries. *Journal of The Electrochemical Society*, 152(1):A255–A263, 2005.

[27] A. Reid, S. Langer, R. Lua, V. Coffman, S. Haan, and R. García. Image-based finite element mesh construction for material microstructures. *Computational Materials Science*, 43(4):989–999, 2008.

[28] A. Reid, R. Lua, R. García, V. Coffman, and S. Langer. Modelling microstructures with OOF2. *International Journal of Materials and Product Technology*, 35(3):361–373, 2009.

[29] D. Chandrasekharaiah and L. Debnath. *Continuum mechanics*, chapter 9.2. Academic Press, San Diego, 1994.

[30] B. Harris. *Engineering Composite Materials*. Institute of Materials, London, 1999.

[31] M. Griebel, S. Knapek, and G. Zumbusch. *Numerical Simulation in Molecular Dynamics: Numerics, Algorithms, Parallelization, Applications*. Springer, 2007.

[32] J. Wang and R. Pyrz. Prediction of the overall moduli of layered silicate-reinforced nanocomposites–part I: basic theory and formulas. *Composites Science and Technology*, 64(7):925–934, 2004.

[33] G. Tandon and G. Weng. The effect of aspect ratio of inclusions on the elastic properties of unidirectionally aligned composites. *Polymer Composites*, 5(4):327–333, 1984.